

1 **Appendix A: Site-specific Measurement Techniques**

2 Site-specific isotope ratios of alanine derivatives are measured on the Orbitrap Fourier
3 Transform Isotope Ratio Mass Spectrometer ('Orbitrap'). Prior studies have demonstrated that
4 the fragments of alanine N-trifluoroacetyl-O-methyl ester can full constrain the C-1, C-2, and C-
5 3 sites of alanine (Eiler et al., 2017; Chimiak et al., 2020); here we detail the peak analyzed, the
6 conditions in which the Orbitrap measurements in this study were performed, and the rationale
7 for those conditions.

8
9 The Orbitrap has two front-end configurations, dual- and single-reservoir. Measurements for
10 fragment verification typically used the dual-reservoir configuration depicted in Figure S1. This
11 configuration has two reservoirs with a pure sample in one and a standard in the other that elutes
12 into the instrument by a helium stream and a front valve (V2) that can change which reservoir
13 elute to the source and which to the vent. Measurements of alanine for this study are made using
14 the single-reservoir system, which operates similarly to an exponential dilution flash and is
15 depicted in Figure S1b. In this study, the reservoir consists of a 30 mL steel reservoir coated with
16 deactivated silica. The single reservoir system has two valves. The first valve (V1) has inputs
17 from the GC column and from a capillary attached to the helium tank by way of a pressure
18 regulator, and outputs are either directed to the second valve (V2) or to the reservoir. V2 has
19 inputs from the V1 and the reservoir and outputs to either the Orbitrap source or to vent.

20
21 In single-reservoir analyses, samples are injected into the GC injection port and can be measured
22 as directly as they elute from the GC ('GC direct mode') or they can be selected and broadened
23 in a reservoir ('peak broadening mode'). In this study, the GC is set to start at 50 °C and ramp at
24 10 °C/minute with a helium flow rate of 1.2 mL/min and have a splitless injection. In both GC
25 direct and peak broadening mode, the initial valve set-up routes pure helium from a tank is
26 directed to the reservoir and the reservoir is directed to the Orbitrap source (the GC eluent is
27 directed to vent).

28

29 In GC direct mode, alanine is injected into the Orbitrap and the initial valves are unchanged for 4
30 minutes while the solvent, hexane, elutes as a failure to vent the solvent creates large
31 backgrounds. After four minutes, GC eluent is routed directly to the Orbitrap source. This mode
32 was used on large mass windows (50-500 Da) to note elution times and find potential fragments
33 using labelled alanine standards and daily on a smaller mass windows (± 5 Da) to confirm that the
34 elution time was unchanged and that there was low contamination.

35
36 In peak-broadening mode, helium is routed to the reservoir and source for the first 6.0 minutes
37 (Figure S2) as alanine elutes at 7.5 minutes. At this time, the GC eluent is routed to the reservoir,
38 which is routed to the Orbitrap source. At 11 minutes—after which the full alanine peak has
39 eluted—helium is routed to the reservoir for the remainder of the acquisition. All isotope ratio
40 measures for the C-2 and C-3 sites of alanine reported here are measured in peak-broadening
41 mode, in which the alanine peak was captured and measured for 60-minutes per injection.

42
43 The path of the sample from the GC front-end to the Orbitrap and its potential impacts on the
44 isotopic measurements is described at length in Eiler et al. (2017). Once gas enters the electron
45 impact (EI) source, electrons from the source impact the analyte and break chemical bonds
46 and/or remove electrons to produce charged fragments. These fragments are then collimated into
47 a beam and filtered by their mass-to-charge ratio via the Advanced Quadrupole Selector
48 (AQS)—a quadrupole mass selector. Typically, fragments have a +1 charge, so the mass-to-
49 charge ratio corresponds to the fragments' mass. We will refer to the mass range that is filtered
50 in the quadrupole as the 'mass window'. Ions in the mass window are collected in an
51 electrostatic trap (C-trap) until a user-defined threshold for the total ion current (TIC) in the C-
52 trap is reached. This threshold measured via the automatic gain control (AGC). Once the TIC in
53 the C-trap reaches the threshold, ions are injected from the C-trap into the Orbitrap where they
54 oscillate and travel back and forth in the Orbitrap at a rate proportional to mass (Makarov, 2000).
55 The time the ions spend in the C-trap prior to injection is referred to as the injection time (IT). If
56 the TIC in the C-trap remains below the threshold for a user-defined amount of time (the max
57 IT), the ions are injected into the Orbitrap and measured. We refer to these scans as ones in

58 which the IT is ‘maxed out.’ We refer to each process of injecting an ion packet into the Orbitrap
59 and measuring it in this manner as a scan and the combination of scans that forms a measurement
60 as an acquisition. Using Excalibur, a proprietary software program by Thermo Fisher Scientific,
61 the frequency signal produced by the back and forth travel of ions is deconvolved via a Fourier
62 Transform function and the mass and signal intensity of the ions is reported to a user for each
63 scan in an acquisition. Following acquisitions, all data files are processed through a proprietary
64 software program provided by Thermo Fisher Scientific, ‘FT statistic’, which extracts
65 information from a RAW file including intensity, peak noise and total ion counts for each scan
66 pertaining to requested masses and converts them into a .csv file. Following extraction in FT
67 statistic, isotopic intensities are converted to counts according to Eiler et al. (2017).

68
69 Fragmentation by electron impact is a high energy process, so we anticipate potential
70 recombination reactions occur within the source that could impact the sites that are sampled by
71 each fragment. The carbon sites included in fragments are identified by using a 1:9 mixture of
72 ¹³C-labelled alanine (at the C-1, C-2, or C-3 site) with unlabeled alanine that is derivatized into a
73 N-trifluoroacetyl-O-methyl ester and diluted to 1:100,000 (parts per volume) in hexane and
74 injected through the GC into the Orbitrap for initial fragment identification. With this analysis,
75 we recognize candidate fragments listed in Table S1 and further explore which alanine sites
76 contribute 102.055, 113.021, 140.032, 184.021, and 200.053 fragments and their ¹³C-substituted
77 versions. For this paper, we will refer to pairs of fragments by the monoisotopic fragment’s
78 mass.

79
80 Fragments-of-interest were further analyzed using the 1:9 labelled standards in dual-reservoir
81 mode for the 102.055, 140.032, 184.021, and 200.053 fragments and single-reservoir mode for
82 the 113.021 peak. In these analyses, if a fragment contained 100% of the C-1 site, the C-1
83 labeled compound would have a $\delta^{13}\text{C}$ that is 11500 ‰ to 2800 ‰ enriched relative to the
84 unlabeled alanine standard for a fragment that contains one to five carbons, respectively. Results
85 from single- and dual-reservoir measurements of the labelled peaks demonstrate that the 102.055
86 fragment contains the C-3 site and two derivative carbons, the 113.021 fragment contains the C-3

87 site and two derivative carbons, the 140.032 fragment contains the C-2 and C-3 sites in addition
88 to two derivative carbons, the 184.021 fragment contains the C-1 and C-2 carbons in addition to
89 three derivative carbons, and the 200 and 201 fragments contain all three carbons in alanine and
90 all three derivative carbons (Table S2). In each case, fragments returned either 0% or 100% of a
91 given site's label.

92
93 To test Orbitrap acquisition parameters, Alfa Aesar and Strecker alanine standard derivatives
94 were analyzed in dual-reservoir acquisitions. These standards have known $\delta^{13}\text{C}_{\text{VPDB}}$ values for
95 the C-1 site via ninhydrin decarboxylation, whole molecule $\delta^{13}\text{C}_{\text{VPDB}}$ from EA measurements,
96 and the $\delta^{13}\text{C}_{\text{VPDB}}$ averaged across the C-2 and C-3 sites via subtraction. Parameters included
97 AGC, microscans, resolution, and window size (Table S3) were varied. At best, Dual reservoir
98 studies find the following structure of Strecker alanine relative to Alfa Aesar $-17.0 \pm 8.6 \text{ ‰}$, -9.8
99 $\pm 3.9 \text{ ‰}$, and -21.2 ± 1.4 for the C-1, C-2, and C-3 sites, respectively, and the error follows the
100 shot noise limit. For mass windows and fragments considered, only measurements with AGC
101 values below 1×10^5 ions accurately replicate the differences between Strecker and Alfa Aesar
102 alanine, so we adopt this AGC value for the measurements presented in this study. Higher
103 resolution and smaller scan windows decreased the ion transmission (Eiler et al., 2017), so
104 120,000 resolutions are used to ensure the full separation of the singly-substituted ^{13}C and ^{15}N
105 peaks for the masses studied here and scan windows of ± 5 Da were used to decrease possible
106 contaminant peaks while still keeping transmission high. Differences in microscans do not
107 impact the data, so we use 1 microscan to monitor potential noise.

108
109 Measurement of the Alfa-Aesar and Strecker standards with the single-reservoir front-end,
110 demonstrate how IT and timing for peak capture. Data from scans that were conducted at
111 maximum IT were highly fractionated, so in for acquisitions in this study, maximum IT is set to
112 3000 ms and scans in which the IT maxes out are culled prior to data processing. Peaks are
113 captured in the reservoir via manual valve control. To decrease background, peak should be close
114 to when they elute; however, the strong ^{13}C fractionation along a GC column that might result in
115 the closer valve turns to miss small amounts of the eluted analyte in an inconsistent fashion. Here

116 we find that acquisitions in which the valve is turned at least before 30s prior to the peak's
117 elution have relative ^{13}R values within 2 standard error, but the acquisitions have a larger as
118 peaks are captured closer to their elution (Table S4). Consequently, measurements here capture
119 alanine peaks from 6.5 minutes to 11 minutes.

120
121 Finally, we analyzed the acquisition data for the Alfa Aesar and Strecker alanine standard
122 derivatives by processing the ^{13}R values as an average for the acquisition, an average weighted
123 by counts per scan, an average weighted by TIC of each scan, and the summed singly ^{13}C -
124 substituted peak counts over the monoisotopic peak counts for each acquisition. In each analysis,
125 we further culled each data set according to its peak height (from no culling to culling all scans
126 with the monoisotopic peak at or below 50% of its peak maximum less the background) and
127 according to its monoisotopic peak intensity relative to the TIC (from no culling to culling all
128 scans with the monoisotopic peak intensity at or below 50% of the TIC). For the sample sizes
129 here on the 140.035 Da peak, only analyses in which no cutoffs were used were found to have
130 values that were one standard deviation from the C-2 + C-3 value (Table S5). As the ^{13}R value
131 for the 140.035 Da peak is both most accurate and most precision for a cutoff of the
132 monoisotopic peak's intensity being at least 30% of the TIC for a scan and when calculating ^{13}R
133 as an average weighted by the counts per scan (Table S5), we adopt this as our culling criteria in
134 data processing.

135

136 **Appendix B: Ninhydrin Decarboxylation**

137 Ninhydrin cleaves amino acids' carbon (the C-1 site), which becomes CO_2 (Donald D. Van
138 Slyke et al., 1941). The ninhydrin reaction followed by capture of the produced CO_2 provides a
139 sample on which to measure an amino acid's $\delta^{13}\text{C}$ of the carboxyl site (the C-1 site) (Abelson
140 and Hoering, 1961). We measure the CO_2 produced from the ninhydrin reaction of alanine on an
141 IRMS to constrain $\delta^{13}\text{C}$ of the C-1 site for the three alanine standards (See Materials: Alanine
142 Standards).

143

144 The ninhydrin reaction (D D Van Slyke et al., 1941) is performed in a custom-made 50 mL
145 borosilicate flask (Figure S3) with one sealable port that attaches to a custom-built gas-line (used
146 similarly to a Schlenk-line in this study) and one port that has a Swagelok fitting and septum.
147 The gas-line has two in-line water traps and two pressure gauges, which enable pressure readings
148 from 1.00×10^{-3} mTorr to 760 Torr. The ninhydrin decarboxylation follows methods adapted
149 from Van Slyke et al. (1941). In short, we add 57 mg of ninhydrin, 15 mg alanine, and 92 mg
150 citric acid (exact quantities in Table S6) to a custom-made borosilicate flask. This flask is then
151 attached to a gas-line via a Swagelok with a frit to avoid solid materials from entering the line
152 and is then evacuated. While the flask is being evacuated, 10 mL water is added to a 40 mL vial
153 that is subsequently capped. Helium is bubbled through the water for 10 minutes to remove any
154 carbon dioxide. Once the flask is evacuated (0.005 mTorr or below as read by the pressure
155 gauge), both the port to the reaction flask and to the gas-line are closed. The flask is taken off the
156 line and placed in a fume hood where 5 mL of degassed water is injected into the vial through the
157 septum. The flask is then placed in an ethylene glycol bath at 100 °C for 32 minutes after which
158 it is removed from heat and connected to the gas-line. The flask is placed in a -15 °C ethylene
159 glycol-dry ice bath for 20 minutes or until all liquid in the flask is frozen, whichever is longer.
160 During this time, a borosilicate tube is attached to another port on the Gas-line, evacuated, and
161 the port to it is closed. Once the contents of the reaction vessel are frozen, the ports to the pumps
162 are closed and those to the reaction vessel are opened and the pressure is recorded. One of the
163 water traps is then submerged in an ethanol-dry ice bath for 5 minutes or until the pressure
164 reaches 0.005 mTorr. At this point, the port to the reaction vessel is closed, the ethanol-dry ice
165 bath is removed, and the gas equilibrates in the line. We record the pressure, open the port to the
166 borosilicate tube, and immerse the tube in liquid nitrogen. One minute after the pressure reaches
167 0.005 mTorr, the tube is sealed with a O₂ torch.

168

169 Once trapped in a borosilicate tube, CO₂ is measured by IRMS on a Thermo Fisher Delta V with
170 two ethanol-dry ice traps and a GC on the front end for sample purification. To introduce sample
171 into the instrument, borosilicate tubes are scored, and the scored end is sealed into a flexible
172 metal tube via a Swagelok. The other end of the metal tube has a second Swagelok with a frit on

173 it—this Swagelok is attached the purification line on the front end of the Delta V. After
174 evacuating inlet to the tube, a line is open between it and the first gas trap and the tube is broken.
175 Gas equilibrates for one minute before the inlet port is shut. Measurements of CO₂ for each
176 sample is measured in dual-inlet mode against a CO₂ standard with a known $\delta^{13}\text{C}_{\text{VPDB}}$
177 composition.

178

179 The C-1 site of three alanine samples are constrained using ninhydrin decarboxylation. The
180 $\delta^{13}\text{C}_{\text{VPDB}}$ of the C-1 sites for Alfa Aesar and VWR alanine standards are nearly equal at $-28.5 \pm$
181 0.1 ‰ and $29.6 \pm 0.1 \text{ ‰}$, respectively. The Strecker alanine standard's C-1 site has a $\delta^{13}\text{C}_{\text{VPDB}}$
182 of $-43.5 \pm 0.1 \text{ ‰}$, which approximately 15 ‰ below that of the other standards (Eiler et al.,
183 2017). These $\delta^{13}\text{C}$ values of the C-1 sites are invariant with respect to yield, reaction time, or the
184 proportion of ninhydrin to alanine. Combining the $\delta^{13}\text{C}_{\text{VPDB}}$ of the C-1 sites of alanine with the
185 molecular-average $\delta^{13}\text{C}_{\text{VPDB}}$ measurement, we calculate $\delta^{13}\text{C}_{\text{VPDB}}$ for the averaged C-2 and C-3
186 sites for all three standards as well (Table S6).

187

188 **Appendix C: Equilibrium calculations**

189 The equilibrium constants for the reactions that occur during the equilibration step provide a
190 means to estimate the proportions of species at intermediate steps that we have not directly
191 analyzed. These concentrations include the equilibrium concentration of α -aminopropanenitrile
192 (α -APN), ammonia, acetaldehyde, and cyanide. Equilibrium concentrations of these species are
193 solved for in a series of equilibrium, water activity, and mass balance equations. Equations S1 to
194 S8 are equilibrium equations that relate the relative concentrations of products and reactants to
195 the known values of equilibrium constants (*i.e.*, the ratio of forward and reverse reactions, listed
196 in Table S5) for reactions in which those products and reactants participate (Eqn. S1 to S14).
197 Equation S9 calculates the water activity at the end of the equilibrium step. Equations S10 to S14
198 are mass balance equations, which assert that the number of moles of an element of interest
199 contained in a specific pool of initial reactants (e.g., the N atoms in ammonium chloride) at the
200 start of the equilibration step (here denoted with a $t = 0$ subscript) must equal the number of
201 moles of that element contained in the residual pool of those reactants plus the number of moles

202 of that element that were transferred to products at the end of that step (note: no subscript is used
 203 for the concentrations at the end of equilibrium).

204

$$205 \quad K_1 = \frac{[\text{NH}_3][\text{H}^+]}{[\text{NH}_4^+]} \quad (\text{Eqn. S1})$$

206

$$207 \quad K_2 = \frac{[\text{CN}^-][\text{H}^+]}{[\text{HCN}]} \quad (\text{Eqn. S2})$$

208

$$209 \quad K_3 = \frac{[\text{CH}_3\text{CHO}] \cdot a_1}{[\text{CH}_3\text{CH}(\text{OH})_2]} \quad (\text{Eqn. S3})$$

210

$$211 \quad K_4 = \frac{[\text{CH}_3\text{CH}(\text{NH}_2)\text{CN}][\text{OH}^-]}{[\text{NH}_3][\text{CN}^-][\text{CH}_3\text{CHO}]} \quad (\text{Eqn. S4})$$

212

$$213 \quad K_5 = \frac{[\text{CH}_3\text{CH}(\text{NH}_2)\text{CN}][\text{H}^+]}{[\text{CH}_3\text{CH}(\text{NH}_3^+)\text{CN}]} \quad (\text{Eqn. S5})$$

214

$$215 \quad K_6 = \frac{[\text{CH}_3\text{CH}(\text{O})\text{CN}]}{[\text{CN}^-][\text{CH}_3\text{CHO}]} \quad (\text{Eqn. S6})$$

216

$$217 \quad K_7 = \frac{[\text{CH}_3\text{CH}(\text{O})\text{CN}][\text{H}^+]}{[\text{CH}_3\text{CH}(\text{OH}^+)\text{CN}]} \quad (\text{Eqn. S7})$$

218

$$219 \quad K_8 = \frac{[\text{H}^+][\text{OH}^-]}{a_1} \quad (\text{Eqn. S8})$$

220

$$221 \quad a_1 = \frac{n_{\text{H}_2\text{O}}}{n_{\text{CN}} + n_{\text{HCN}} + n_{\text{CH}_3\text{CHO}} + n_{\text{CH}_3\text{CH}(\text{OH})_2} + n_{\text{NH}_3} + n_{\text{NH}_4} + n_{\text{CH}_3\text{CH}(\text{NH}_2)\text{CN}} + n_{\text{CH}_3\text{CH}(\text{NH}_3^+)\text{CN}} + n_{\text{CH}_3\text{CH}(\text{O})\text{CN}} + n_{\text{CH}_3\text{CH}(\text{OH})\text{CN}}$$

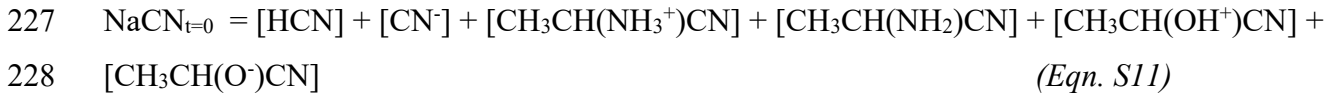
$$222 \quad (\text{Eqn. S9})$$

223

$$224 \quad [\text{NH}_4\text{Cl}]_{t=0} = [\text{NH}_4^+] + [\text{NH}_3] + [\text{CH}_3\text{CH}(\text{NH}_3^+)\text{CN}] + [\text{CH}_3\text{CH}(\text{NH}_2)\text{CN}]$$

$$225 \quad (\text{Eqn. S10})$$

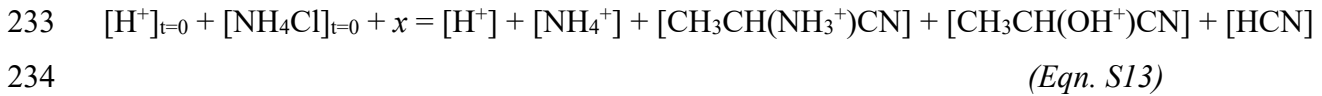
226



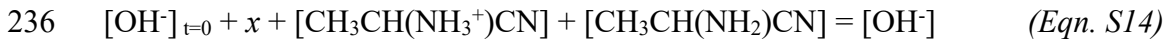
229



232



235



237

238 The variable x is defined below.

239

240 This system of equations accounts for all possible species in solution during the equilibrium step.
 241 Initial masses of ammonia and cyanide were weighed and recorded, and volumes of acetaldehyde
 242 and water were measured in syringes and recorded from each synthesis (Table 1, main text). For
 243 the equation 16, OH^- sources consist of initial OH^- , OH^- produced when α -APN is formed, and
 244 OH^- produced from water dissociation. This final OH^- source is denoted as x and accounts for the
 245 degree of auto-dissociation of water: because the equilibrium constant for water dissociation at a
 246 given temperature is always equal to the product of the concentration of H^+ and OH^- divided by
 247 the water activity (a_l) (Eqn. S9)—the partial vapor pressure of water in a solution relative to that
 248 of pure water, which is roughly equal to 0.98 in our system as defined by equation 12— x is the
 249 change in $[\text{H}^+]$ and $[\text{OH}^-]$ from water formation or dissociation that must occur to satisfy
 250 equation 11. Gas phase concentrations of reactants were negligible (<0.1%), so we did not
 251 include these in our model. Initial water is assumed to have a pH of 7. When calculations were
 252 repeated at a pH of 5.6 to account for the uptake of CO_2 from air, the results were within error of
 253 those presented here.

254

255 **Appendix D: Calculation of α -APN formation and degradation during H-1**

256

257 The α -APN formation and decomposition reactions are the forward and reverse components of
258 reaction 4, respectively (Table S5). We solve for their separate rates using equations 18 and 19
259 and rate constants from Van Trump (1975) (Table S5):

260

$$261 \quad v_{fwd} = k_{f1} * \frac{[RCHO][CN^-][NH_3]}{[OH^-]} \quad (Eqn. S15)$$

262

$$263 \quad v_{rev} = k_{r1} * [\alpha\text{-APN}] \quad (Eqn. S16)$$

264

265 In these equations, v_{fwd} is the rate of α -APN production from reactants (acetaldehyde, cyanide,
266 and ammonia), and v_{rev} is the rate of α -APN decomposition into reactants. Rate constants k_{f1} and
267 k_{r1} (Table S5) are for the reaction rate for the forward and reverse reactions, respectively. The
268 forward and reverse velocities depend on the concentrations α -APN, CN^- , NH_3 , and OH^- , all of
269 which are pH dependent, so we solve equations 18 and 19 for two pH conditions, the pH value at
270 the end of equilibrium (pH = 8.2), which we solve for above, and the pH value during hydrolysis
271 (pH < 1).

272

273 The quantities $[NH_3]$, $[CN^-]$, and $[\alpha\text{APN}]$ present at the beginning of the hydrolysis step for the
274 two pH conditions listed above are calculated using the relationship:

275

$$276 \quad [base] = [acid + base] * \frac{K_a}{K_a + [H^+]} \quad (Eqn. S17)$$

277

278 where [base] is the concentration of the basic species of a compound of interest, [acid + base] is
279 the total concentration of that compound in solution, and K_a is the acid dissociation constant for
280 the compound (Table S5). In the case of ammonia, [base] is $[NH_3]$, [acid + base] is $[NH_4^+ +$
281 $NH_3]$, and K_a equals $K_{a,NH4}$, which equals 5.6×10^{-10} (Table S5).

282

283

284 **Appendix E: Calculation of isotope effects**

285

286 Isotope effects on nitrogen for the equilibrium step are calculated using equation S18 (subscripts
287 refer to the molecule of interest of f_x and $^{15}F_x$ values and refer to the product/reactant for the α
288 values):

289

$$290 \quad ^{15}F_{tot} = \frac{f_{NH_3}}{1 + \alpha_{\alpha APN} \left(\frac{1}{^{15}F_{\alpha APN}} - 1 \right)} + \frac{f_{NH_4} \frac{\alpha_{NH_4}}{NH_3}}{\alpha_{NH_4} + \alpha_{\alpha APN} \left(\frac{1}{^{15}F_{\alpha APN}} - 1 \right)} + f_{\alpha APN} ^{15}F_{\alpha APN}$$

291

(Eqn. S18)

292

293 where $^{15}F_{tot}$ is calculated from the $\delta^{15}N$ value of ammonia added to the reaction vessel and
294 $^{15}F_{\alpha APN}$ is the ^{15}F value of the α -APN pool at equilibrium, which is assumed to be equal to the ^{15}F
295 value of final product alanine, as ^{15}F does not change significantly and consistently with the
296 reaction progress of steps H-1 or H-2 (see Results). The f_x values in equation S18 are the
297 fraction of compound x at equilibrium and are equal to the concentration of x calculated at
298 equilibrium divided by the concentration of NH_4Cl added to the reaction vial. The $\alpha_{P/R}$ values for
299 nitrogen, defined as the ratio of $^{15}R_P/^{15}R_R$, are equilibrium isotope fractionations between the
300 product (subscript P) and the reactant (subscript R; ammonia in this case). We use a value of
301 1.029 for α_{NH_4/NH_3} (Walters et al., 2019).

302

303 Isotopic compositions for the carbon atoms that will ultimately be transferred to the C-2 and C-3
304 sites of alanine are calculated for the equilibrium step with equation S19:

305

$$306 \quad ^{13}F_{tot} = \frac{f_{ace}}{1 + \alpha_{\alpha APN} \left(\frac{1}{^{13}F_{\alpha APN}} - 1 \right)} + \frac{f_{ace(OH)_2} \frac{\alpha_{ace(OH)_2}}{ace}}{\alpha_{ace(OH)_2} + \alpha_{\alpha APN} \left(\frac{1}{^{13}F_{\alpha APN}} - 1 \right)} + f_{\alpha APN} ^{13}F_{\alpha APN}$$

307

308

(Eqn. S19)

309

310 Equation S19 is analogous to equation S18 but considers the carbons transferred from
311 acetaldehyde to α APN. In equation S19, $^{13}F_{tot}$ is based on the molecular average $\delta^{13}C$ value of
312 acetaldehyde added to the reaction vessel and $^{13}F_{\alpha APN,eq}$ is the ^{13}F value of the carbons in α -APN
313 that will become C-2 and C-3 in alanine. Each f_x value is the concentration of compound x at
314 equilibrium for a specific experiment divided by the concentration of acetaldehyde initially
315 added to the reaction vial for that experiment. Here the compounds are abbreviated as follows:
316 acetaldehyde is 'ace', acetaldehyde hydrate is 'ace(OH)₂', and α -APN is α APN. The $\alpha_{P/R}$ values
317 are as defined in the preceding paragraph but for ^{13}R instead of ^{15}R . As there are no
318 measurements of the equilibrium carbon isotope effect between acetaldehyde and acetaldehyde
319 hydrate, we adopt a value of 1.0034 for $\alpha_{ace(OH)_2/ace}$, which is half the value for CO₂ hydration a it
320 would be averaged over two carbons in acetaldehyde (Marlier and O'Leary, 1984).

321
322 The equilibrium concentrations calculated in equations 4 to 17 find that effectively all (> 95 %)
323 cyanide added at the start of an experiment is transferred to the C-1 site of α -APN (with the
324 remainder being transferred to the C-1 site of α -hydroxypropionitrile). α -APN and
325 α -hydroxypropionitrile have the same bonding environment at the C-1 site and therefore we
326 adopt the approximation that they have the same equilibrium carbon isotope effects with respect
327 to cyanide. Consequently, we can assert that the C-1 site of α -APN (and α -hydroxypropionitrile)
328 has a $\delta^{13}C$ value at equilibrium closely similar to that of initial HCN reagent. However, we do
329 not have an estimate of the equilibrium fractionation factor between HCN and α -APN (and
330 α -hydroxypropionitrile), and thus we cannot assign a value to the $\delta^{13}C$ of the trace of residual
331 CN at the end of the equilibrium step; however, this uncertainty has no impact on our ability to
332 predict or interpret $\delta^{13}C$ values of other species of interest.

333
334 Our experimental results (detailed below) indicate negligible isotopic fractionation of the carbon
335 atoms that will end up in the C-2 and C-3 sites of alanine during the H-2 reaction step because
336 the $\delta^{13}C$ value of these sites are approximately invariant across the progress of this irreversible
337 reaction. This implies that H-2 has negligible secondary and tertiary carbon isotope effects.
338 Consequently, we can use the ^{13}F value for the C-2 and C-3 sites in product alanine and assume

339 they are the same for initial alaninamide and with these values calculate the ^{13}F and therefore ^{13}R
340 values at the C-1 site in alaninamide and alanine according to equation 3. Combining these C-1
341 site ^{13}R values and with that of the α -APN's C-1 site provides the ^{13}R values for all of the
342 reactants and products in H-1 and H-2. These values enable us to calculate the isotope effect for
343 H-1 and H-2 by using the Rayleigh equation, written below in equation 23, for each hydrolysis
344 step separately.

345

$$346 \quad f^{\frac{\alpha_P-1}{R}} = \frac{{}^{13}\text{R}_R}{{}^{13}\text{R}_{R,0}} \quad (\text{Eqn S20})$$

347

348 where $^{13}\text{R}_R$ and $^{13}\text{R}_{R,0}$ are the ^{13}R values for the residual and initial reactants (α -APN for H-1 and
349 alaninamide for H-2), f is the fraction of residual to initial reactant, and $\alpha_{P/R}$ is fractionation
350 factor between the product and reactant.

351

352 Finally, we calculate molecular-average isotope fractionations for the equilibrium step, H-1, and
353 H-2. As the CN is calculated to have nearly quantitative incorporation into the intermediate α -
354 APN, the equilibrium isotope effect for the full molecular average can be calculated as 2/3 times
355 that of the acetaldehyde's equilibrium isotope effect with α -APN's averaged C-2 and C-3 sites.
356 The molecular-average isotope effects at H-1 are calculated using the Rayleigh equation (Eqn.
357 S20) with α -APN's calculated molecular-average ^{13}R values and the initial alaninamide's
358 calculated ^{13}R values. Finally, the molecular-average isotope effects at H-2 are similarly
359 calculated from the Rayleigh equation (Eqn. S20) and the calculated initial ^{13}R for alaninamide
360 and measured ^{13}R of alanine.

361

Bibliography

- Abelson P. H. and Hoering T. C. (1961) Carbon isotope fractionation in formation of amino acids by photosynthetic organisms. *Proc. Natl. Acad. Sci. USA* **47**, 623–632.
- Chimiak L., Elsila J. E., Dallas B., Dworkin J. P., Aponte J. C., Sessions A. L. and Eiler J. M. (2020) Carbon isotope evidence for the substrates and mechanisms of prebiotic synthesis in the early solar system. *Geochim. Cosmochim. Acta*.
- Eiler J., Cesar J., Chimiak L., Dallas B., Grice K., Griep-Raming J., Juchelka D., Kitchen N., Lloyd M., Makarov A., Robins R. and Schwieters J. (2017) Analysis of molecular isotopic structures at high precision and accuracy by Orbitrap mass spectrometry. *Int. J. Mass Spectrom.* **422**, 126–142.
- Makarov A. (2000) Electrostatic axially harmonic orbital trapping: a high-performance technique of mass analysis. *Anal. Chem.* **72**, 1156–1162.
- Marlier J. F. and O’Leary M. H. (1984) Carbon kinetic isotope effects on the hydration of carbon dioxide and the dehydration of bicarbonate ion. *J. Am. Chem. Soc.* **106**, 5054–5057.
- Moutou G., Taillades J., Bénéfice-Malouet S., Commeyras A., Messina G. and Mansani R. (1995) Equilibrium of α -aminoacetonitrile formation from formaldehyde, hydrogen cyanide and ammonia in aqueous solution: Industrial and prebiotic significance. *J Phys. Org. Chem.* **8**, 721–730.
- PubChem PubChem.
- Schlesinger G. and Miller S. L. (1973) Equilibrium and kinetics of glyconitrile formation in aqueous solution. *J. Am. Chem. Soc.* **95**, 3729–3735.
- Van Slyke D D, DA MacFadyen and Hamilton P. (1941) Determination of free amino acids by titration of the carbon dioxide formed in the reaction with ninhydrin. *J. Bio. Chem.* **141**, 671–680.
- Van Slyke Donald D., Dillon R. T., MacFadyen D. A. and Hamilton P. (1941) Gasometric Determination of Carboxyl Groups in Free Amino Acids. *J. Bio. Chem.* **141**, 627–669.
- Van Trump J. E. (1975) The Strecker synthesis and its prebiological importance. Doctoral dissertation, University of California: San Diego.
- Walters W. W., Chai J. and Hastings M. G. (2019) Theoretical phase resolved ammonia–ammonium nitrogen equilibrium isotope exchange fractionations: applications for tracking atmospheric ammonia gas-to-particle conversion. *ACS Earth Space Chem.* **3**, 79–89.